Hindawi
International Journal of RF and Microwave Computer-Aided Engineering
Volume 2023, Article ID 5644220, 9 pages
https://doi.org/10.1155/2023/5644220

Research Article

Improving the Probability of Stroke Detection inside the Human Head Using Wideband Polarimetric Synthetic Aperture Radar Imaging

Amir H. Naghavi,[1] **Hamid R. Hassani**,[1] **and Daniel Oloumi**[2]

[1]*Department of Engineering, Shahed University, Tehran, Iran*
[2]*Infineon Technology, Austria AG, Villach 9500, Austria*

Correspondence should be addressed to Hamid R. Hassani; hassani@shahed.ac.ir

Received 2 January 2023; Revised 18 February 2023; Accepted 4 March 2023; Published 16 March 2023

Academic Editor: Ali Gharsallah

This paper presents an imaging system based on ultrawideband microwave radars for the detection of bleeding regions and strokes inside the human head. The proposed system is portable and focuses on revealing bleeding areas with unpredictable shapes using polarimetric data acquisition. A custom-designed dual-polarized bowtie patch antenna capable of pumping the UWB pulses inside the patient's head is designed and presented as the biomedical sensor for the system. The antenna dimensions are $25 \times 25\,mm^2$. It mitigates the mismatch between the air and skin needles of any coupling liquid, resulting in safe SAR levels below 0.5 W/kg and wideband operating bandwidth that covers 1.2-4.5 GHz with unidirectional radiations. To collect the raw polarimetric data, an elliptical array of the proposed antenna is formed around the patient's head model that includes 16 elements in direct contact with the phantom. The performance of the proposed method is validated through an imaging scenario with two nonuniform bleeding areas inside the patient head model. The whole structure is simulated with a Gaussian pulse as the excitation using CST Microwave Studio tools. To produce 2D images of the voxel model, the time-domain elliptical synthetic aperture radar (ESAR) imaging algorithm is applied. Accurately detecting the presence and shape of anomalies in reconstructed images using the proposed method demonstrates the efficiency of the proposed system and determines its advantages over single-polarization systems.

1. Introduction

Microwave-based imaging systems have the benefits of being low profile, portable, low cost, and more importantly nonionizing in comparison to other clinical imaging modalities such as magnetic resonance imaging (MRI), X-ray, or computed tomography (CT). In recent years, many research groups have been focused on the development of microwave imaging techniques for the human body with applications in the early detection and diagnosis of various diseases including tumors, cancer, stroke, and internal human head bleeding [1–4]. Radar-based techniques are at the center of attention in the current research for medical imaging applications. This technology has proved its potential for breast as well as head imaging for identifying head abnormalities like tumors, brain strokes, and bleeding [3–6]. Intensity-based radar image algorithms use coherent summation of reflected signals collected from different aperture positions to form an image. This method is well suited for microwave imaging due to relatively simple image processing and wide operating bandwidth. In this procedure, an ultrashort time-domain, ultrawideband pulse is utilized to illuminate the medium under imaging, and the scattered echoes are collected for postprocessing purposes. By proper design of the antenna's package, radar transceivers, and other elements, the imaging system can be made portable and inexpensive and can be used for bedside or ambulance real-time monitoring [3, 6–8].

In this paper, we are focusing on brain imaging using the aforementioned technology. Various prototypes of microwave systems for stroke diagnosis have been proposed in

the published works. For example, the developed imaging system at Chalmers University consists of an array of triangular shape patch antennas mounted on a plastic helmet operating from 0.8 to 1.5 GHz to detect the injured area inside the patient's head and to distinguish between an ischemic and a hemorrhagic stroke [9]. Several antennas and handheld systems have been proposed by researchers at the University of Queensland for brain imaging applications that are claimed to produce high-quality images of a patient's phantoms [1, 10, 11]. The proposed systems have proven the ability to detect bleeding sites in many realistic scenarios. Another system prototype was developed with EMTensor that consists of 177 rectangular waveguide antennas loaded with ceramic and placed in a hemispherical stainless steel chamber capable of producing anomaly detection within the head [12].

Since the antenna and its array configuration play a major role in the success of imaging systems, several types of antennas and arrays for EM head imaging have been proposed in the literature alongside previously mentioned imaging systems [8, 13–15]. Realizing features such as compactness, low profile, body-matched, and directive patterns in such systems is challenging due to antenna size and frequency band limitations [4, 16].

A comprehensive review of the imaging systems so far shows that researchers' teams have focused on developing imaging systems utilizing single polarization in transceivers aiming to detect simple targets such as spheres, cubes, or cylinders. Consequently, they might tend to fail in the detection of realistic scenarios with complex bleeding geometries. For simple shapes, the backscattered waves retain the incident state of polarization, but for complex ones, the energy moves from one polarization to another based on the target sizes, radar cross-section (RCS), and refractive indices. However, no simple relationship exists between the polarization rotation and the particle irregularity. This phenomenon can cause some parts of the targets' shape to remain hidden from the imaging system whose performance is largely dependent on the amount of reflection toward the receiver.

A functional solution to overcome this weakness can be found by using polarimetric data. This means both polarizations are used in the transceiver to collect more raw data from the imaging medium. The most important advantage of dual-polarized over linear polarized one is its robustness and does not lose information from complex targets. Particularly, for near-field radar imaging, with small targets, within tens of millimeters, complex diffractive mediums having information in both polarization will be helpful. Therefore, this work intends to propose a polarimetric radar system to improve the imaging performance for brain imaging in near-field scenarios.

This article is organized as follows: Section 2 describes the design of a miniaturized dual-pole antenna and its performance as a biomedical sensor for near-field imaging of the human head. Section 3 describes the details of the imaging system setups, elements, and configuration. And ultimately, in Section 4, an imaging scenario is presented containing a realistic 3D phantom of the patient's head, a helmet equipped with 16 proposed antennas, and two complex targets representing bleeding regions. Revealing these regions in the reconstructed image of the patient's head model illustrates the capabilities of such a system for future clinical applications.

2. On-Body Dual-Polarized Antenna: Design and Performance

Brain imaging radar systems require compact antennas that can radiate most of the electromagnetic energy into the head medium to guarantee strong echoes could be captured at the receiver side. Since the human head is an extremely lossy medium, the antenna must also operate in specific frequency bands to ensure a reasonable trade-off is achieved between range resolution and penetration depth [4].

A method to effectively improve the reflection coefficient, as well as radiation characteristics of the antenna, is to immerse antennas in a coupling liquid which acts as an impedance-transformer medium between the radiator and the tissue. However, placing the antennas in the coupling liquid makes it impractical/hard to implement a transportable device [3, 8, 15].

In this section, a dual-pole planar microstrip antenna is proposed. Since the body-matched antennas are a great solution to overcome the aforementioned limits, the proposed antenna is an on-body antenna to enhance the impedance matching with the patient's head. These antennas are in perfect contact with the human tissues, and the EM pulses are deposited into the body by avoiding strong echoes caused by the air-skin mismatch. The dual-pole design also satisfies the need of the imaging system to collect the required polarimetric data.

The structure and dimensions of the proposed antenna are shown in Figure 1(a). It is a modified version of a conventional bowtie patch that is fed vertically at the center with a 50 Ω coaxial line. The dual-polarized specification is fulfilled using two different elements oriented in an orthogonal arrangement. The unidirectional radiation pattern is obtained by placing a conductor ground plane on the back side of the substrate. Each arm is loaded with two shorting pins at the open-sided to lower the cut-off frequency and achieve a more compact size [17]. The final structure consists of two FR4 layers that hold the radiating element. These layers provide a robust construction that protects the radiating element from dust, corrosion, and rust in an operating environment. The antenna dimensions are optimized in direct contact with a multilayer planar model of the human head to attain acceptable radiation and return loss performance as shown in Figure 1(b). The final dimension of the optimized structure is presented in Table 1. The multilayer model contains major tissues of the human head with real dispersive dielectric properties [18].

Figure 1(c) shows the antenna return loss for the VP and HP when placed near a 3D realistic head model. As one can observe, for both polarizations, the antenna return loss is about and below 10.0 dB over the 1.2-4.5 GHz frequency band. This will satisfy the required microwave frequency band for the intended head imaging application [4]. The 3D phantom employed in this study was extracted from

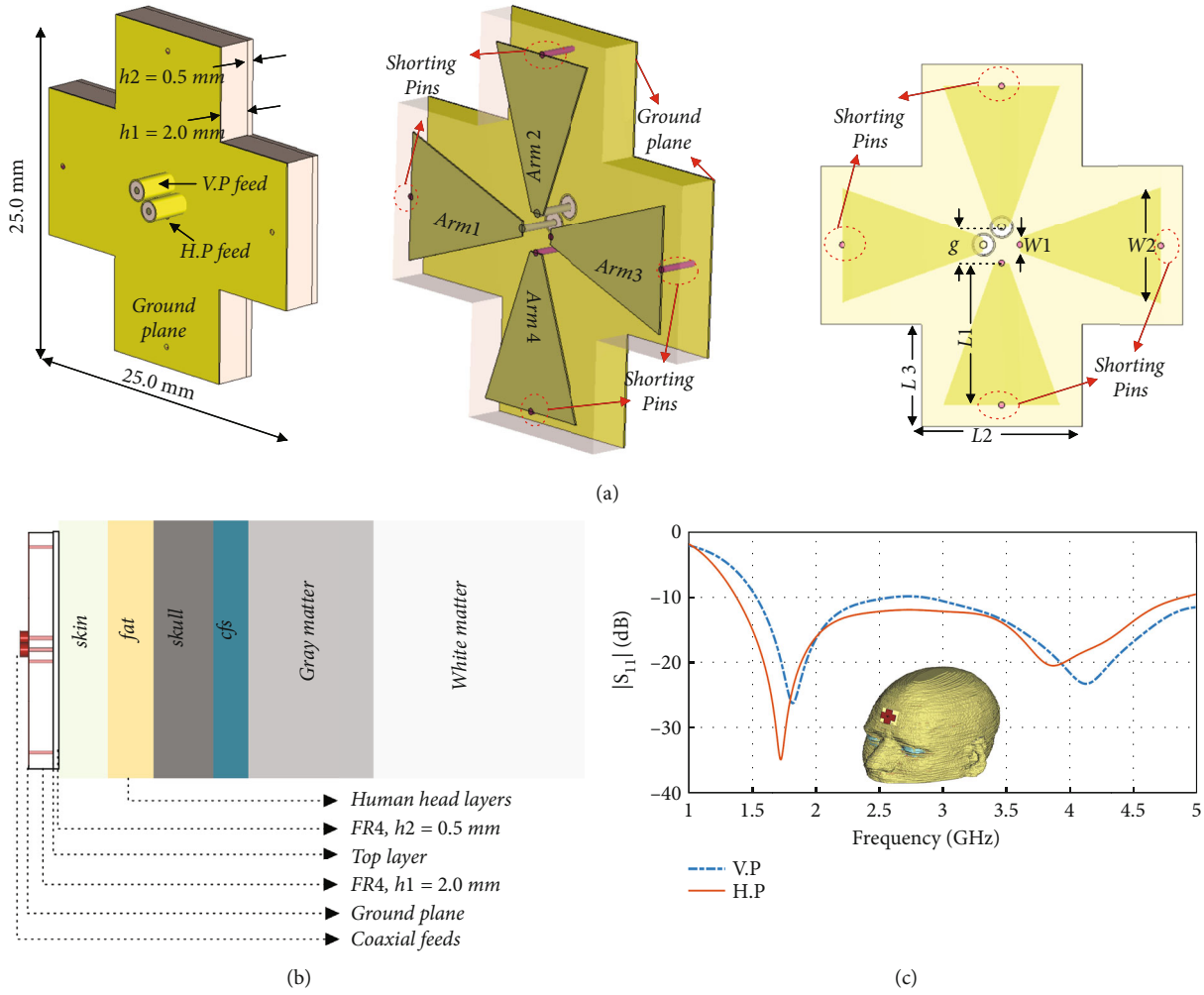

Figure 1: (a) Dual-pole antenna structure, (b) side view of the planar model and antenna, and (c) the reflection coefficient of the dual-pole antenna near the patient's head model.

Table 1: The dimension of the proposed antenna.

Parameters	L1	L2	L3	W1	W2	g
Value (mm)	9.75	11.0	7.0	1.0	8.0	2.5

MRI data of a real patient, which includes major head anatomy layers. The head phantom is voxelized with $256 \times 256 \times 128$ elements with a size of $1.1 \times 1.1 \times 1.4\,\text{mm}^3$ for each element [19]. To simulate the realistic scenario and obtain acceptable results, the measured dielectric parameters (εr and σ) of all tissues over the frequency band are used in the simulator [18].

To discuss the radiation mechanism of the dual-pole antenna, the current density distribution over the operating bandwidth is visualized in Figure 2 using the CST Microwave Studio software. It can be seen that the powerful current, for the most part, is introduced by the coax feed and shorting pins at the end of the bowtie patch which leads to strong current loops flowing through the ground plane and radiating element. This long path generates a resonance in the lower frequency and reduces the overall dimension of the antenna. The orthogonal current distribution is produced by changing the feed of the antenna from VP to HP.

To observe the EM characterization of the proposed antenna in the near-field region, the radiated pointing vector is studied at multiple frequencies as illustrated in Figures 3(a) and 3(b). The pointing vector can estimate the power flow value and the penetration depth of EM pulses at a specific distance from the antenna [20]. The figure depicts that the antenna can successfully pump the electromagnetic power inside the patient's head in both polarizations. A small difference in the penetration depth is observed between VP and HP in some frequencies, which can be caused by the nonuniformity of the 3D model layers or the antenna's arm placement on the forehead in the simulation setup. As can be seen, at higher frequencies, the penetration depth becomes shallower; in this case, frequencies above 4.5 GHz are not useful anymore.

Since the proposed antenna touches the head tissues directly, the specific absorption rate or SAR is a significant consideration to ensure functioning safety when exposed to EM power radiation. The 10 g SAR is determined for various

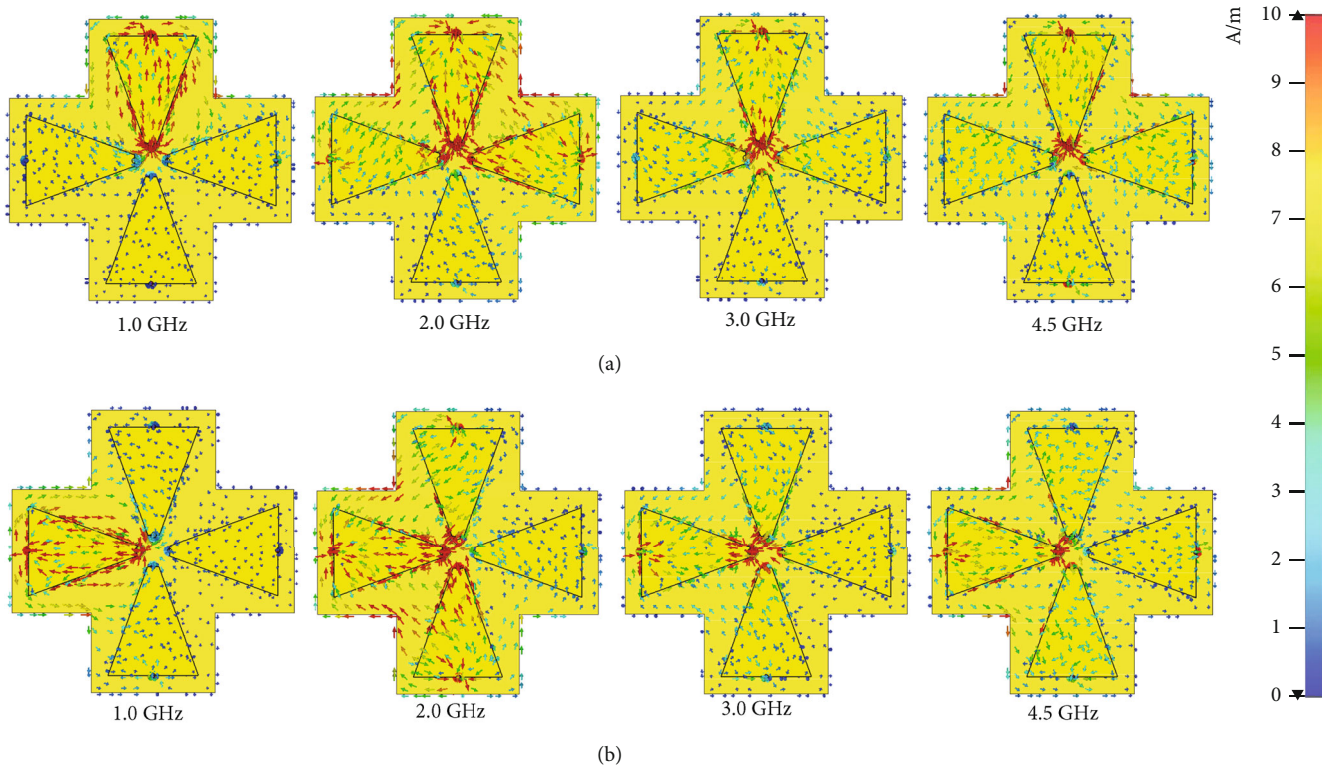

Figure 2: Current density distribution of the proposed antenna. (a) Vertical polarization (VP) and (b) horizontal polarization (HP).

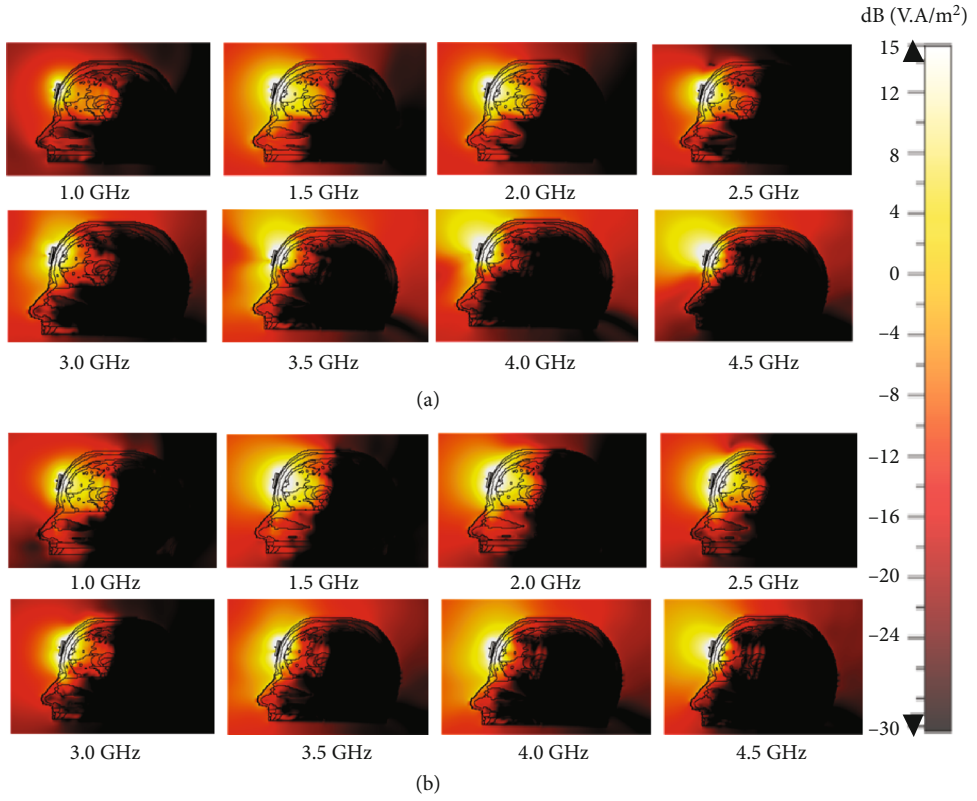

Figure 3: Illustration of the pointing vector over the frequency band. (a) Vertical polarization and (b) horizontal polarization.

frequencies using CST Microwave Studio and the patient's phantom in which the antenna is placed in front of the head. The maximum SAR levels over the frequency band of 1.0-4.5 GHz with a tissue mass of 10 g and 10 dBm input power maintain below 0.5 W/kg as shown in Figure 4. For a UWB monostatic head imaging system, this amount of radiation power can create a safeguard to separate the echo from the noise received [4].

The site of maximum SAR is located almost on the outer layers of the phantom and is mostly distributed on the skin. Even so, the calculated maximum SAR value is well below 1.6 W/kg defined as IEEE public exposure limits [21].

3. The Imaging System Arrangement, Elements, and Algorithms

This section details the arrangement of the UWB imaging system and the image reconstruction method implementing synthetic aperture radar techniques in the time domain. In a later image reconstruction section, the proposed system is validated in realistic scenarios using full-wave simulations of human head phantoms.

3.1. Image Processing Algorithm. The image reconstruction method is based on a global time-domain back projection that shapes the head to fit the elliptical trajectory of data acquisition [4]. This procedure divides the area under investigation into $I \times J$ cells as demonstrated in Figure 5(a). For an elliptical path, the location of the Tx and Rx antennas at each angle can be written as

$$\begin{aligned} X_{\mathrm{Tx/Rx}} &= R(\theta_{\mathrm{Tx/Rx}}).\cos\left(\theta_{\mathrm{Tx/Rx}}\right), \\ Y_{\mathrm{Tx/Rx}} &= R(\theta_{\mathrm{Tx/Rx}}).\sin\left(\theta_{\mathrm{Tx/Rx}}\right), \\ R(\theta_{\mathrm{Tx/Rx}}) &= \frac{A.B}{4 * \sqrt{((A/2).\sin\left(\theta_{\mathrm{Tx/Rx}}\right))^2 + ((B/2).\cos\left(\theta_{\mathrm{Tx/Rx}}\right))^2}}, \end{aligned} \tag{1}$$

with A and B defined as the ellipse dimeters. The reflected signals of scanning antennas are first delayed to focus on a specific spatial point in this area according to the calculated round-trip times, and then, the signals of each antenna within the array are summed for each focal point. The index of the matching sample is found by

$$\mathrm{Index}(I, J) = \frac{D(I, J)}{V_s}, \tag{2}$$

where $D(I, J)$ is written as

$$\begin{aligned} D(I, J) = &\sqrt{\left(X_{\mathrm{Tx}} - X_{(I,J)}\right)^2 + \left(Y_{\mathrm{Tx}} - Y_{(I,J)}\right)^2} \\ &+ \sqrt{\left(X_{\mathrm{Rx}} - X_{(I,J)}\right)^2 + \left(Y_{\mathrm{Rx}} - Y_{(I,J)}\right)^2}. \end{aligned} \tag{3}$$

And V_s is the average propagation speed of light in the imaging medium considered for SAR processing. This procedure is repeated for both polarizations. The sinogram of the recorded raw data through the elliptical path is shown in Figure 5(b). The total image, I_{Total}, is rebuilt through

$$\begin{aligned} I_{\mathrm{Total}} = &\sum_{\theta=0}^{2\pi} \mathrm{rawdata}_{\mathrm{Vertical}}(\theta, \mathrm{Index}(I, J)) \\ &+ \sum_{\theta=0}^{2\pi} \mathrm{rawdata}_{\mathrm{Horizontal}}(\theta, \mathrm{Index}(I, J)). \end{aligned} \tag{4}$$

3.2. Imaging System Elements and Biomedical Sensor Array. Figure 6 depicts the proposed imaging system configuration. The system consists of five basic components: (1) a UWB pulse generator which produces a series of picosecond rising time-step pulses. It contains an impulse-forming network (IFN) excited by a periodic square pulse generator that shapes the output to the first derivative of a Gaussian pulse [22]. The IFN is essential to preserve the deformation of the Gaussian pulse since the antenna cannot radiate its DC component. (2) A sampling oscilloscope that collects the reflected pulses, (3) an RF matrix switch that connects the desired Tx antenna port to the intended receiver antenna port to collect the backscattered pulses, (4) an array of 16 dual-pole biomedical sensors mounted in an elliptical shape trajectory attached directly to the patient's head, and (5) the host computer that controls the matrix switch and stores the raw data to perform the postprocessing algorithms for the image reconstruction.

The transmitted pulse half width is 120 ps corresponding to a center frequency of 2.9 GHz and a -10 dB bandwidth of 4.0 GHz which provides an acceptable performance concerning the range resolution and the penetration depth of microwave pulses within the head medium [4]. To collect the specified polarimetric data, the switch network connects to the relevant TX antenna port and adjacent RX pairs to transmit pulses and collect scattered echoes. This process is repeated with desired specific combinations of TRX to capture raw data from the patient's head. These signals are stored on the host laptop for postprocessing algorithms and image display. To create a 2D image, the raw polarimetric data and the position of the antenna are the inputs of the imaging algorithm. This process must be repeated for another slice of the head for 3D images.

4. Image Reconstruction of the 3D Phantom including Anomalies

4.1. Simulation Scenario Setup. To show the imaging performance of the system and to estimate the merits of such a system in complex scenarios, a full-wave numerical experiment is performed. In this experiment, the bleeding sites inside the patient's head are formed as two nonuniform geometries, an elliptical cylinder, and a torus, with dielectric properties of blood and specific dimensions as shown in Figure 7 [18]. These areas are within the range of minimum dimensions that can be revealed by a radar-based imaging system. A full-wave simulation of this scenario is performed using

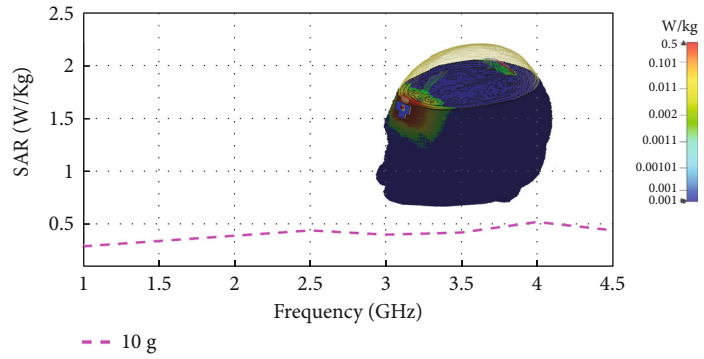

FIGURE 4: The maximum SAR distribution on the patient's head model using the proposed antenna with 10 dBm input power.

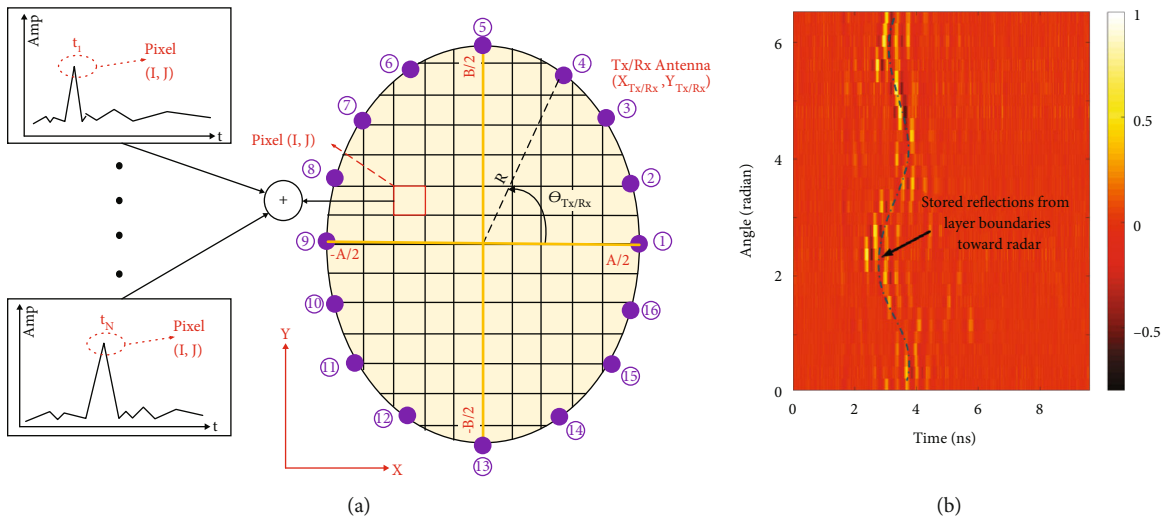

FIGURE 5: (a) Radar trajectory path and (b) collected raw data sinogram.

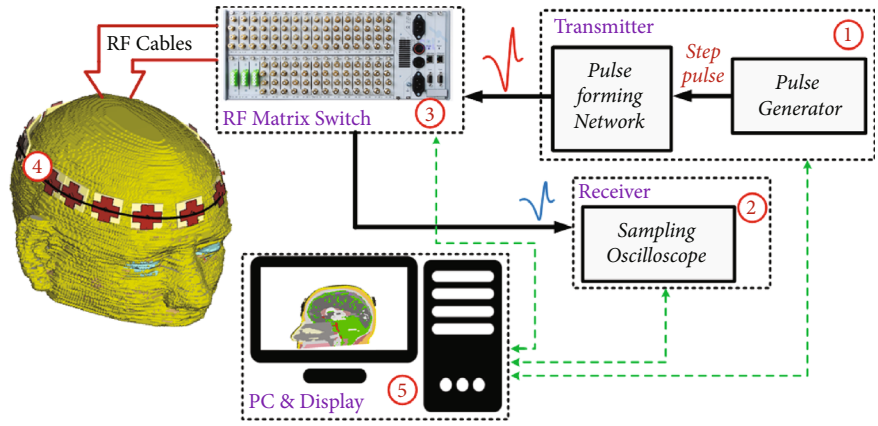

FIGURE 6: Configuration of the imaging system with the antenna array arranged around the patient's head.

time-domain analysis tools in the CST Microwave Studio environment. To establish simulation accuracy, every voxel of the phantom is meshed with at least 20 cells for minimum operating wavelength in each direction in the model which adds up to about 38 million mesh cells.

4.2. Postprocessing and Image Reconstruction. To form the image, two sets of reflected echoes are calculated for each polarization. First, the reflected echoes with the presence of bleeding regions are calculated. Then, the same echoes are calculated by removing the clots from the phantom. These sets of data are

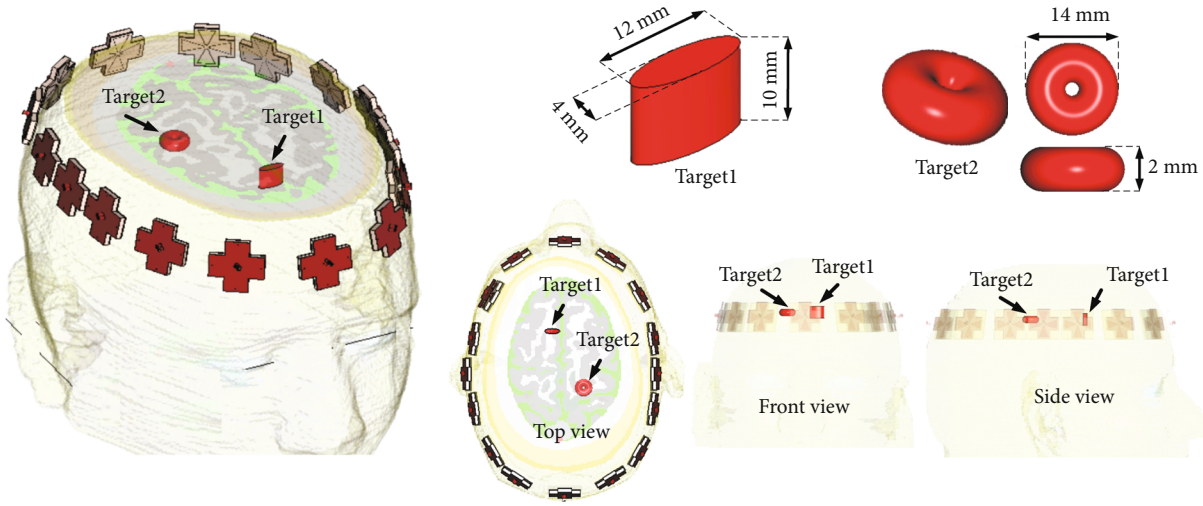

Figure 7: 3D simulation setup phantom with bleeding sites inserted inside the patient's head.

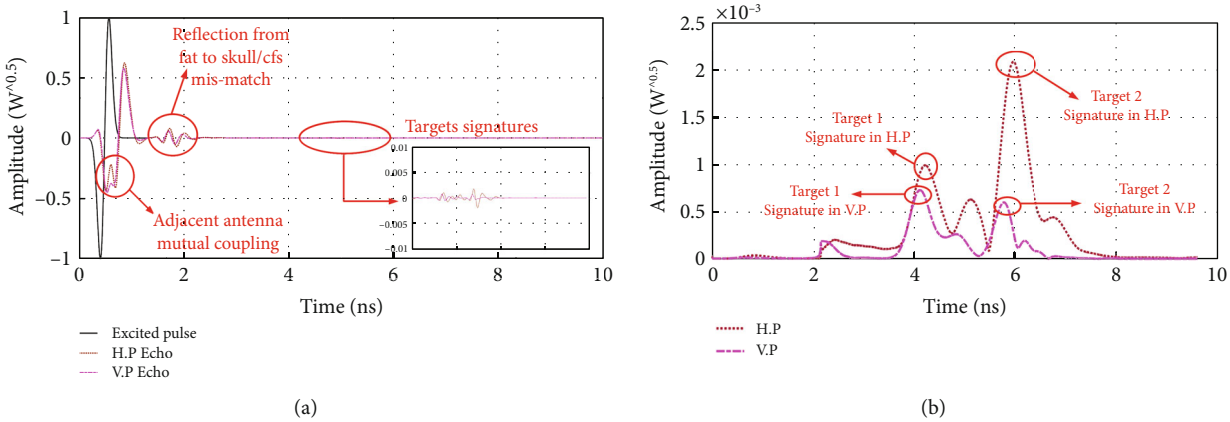

Figure 8: (a) Exciting pulse and reflected echoes and (b) envelope of the calibrated echoes ($\Theta = 0°$).

subtracted to calibrate and eliminate spurious effects, such as the mutual coupling with adjacent antennas [1, 4, 6, 23].

Postprocessing the received pulse can improve the range resolution in synthetic aperture radars. In his work, the received Gaussian pulse is postprocessed by applying a Hilbert transform. Particularly, this transformer would detect the envelope of the received Gaussian pulse [24]. The envelope of the received pulse can be defined as

$$S_{\text{env}}(t) = \text{Abs}(S_r(t) + j.H\{S_r(t)\}). \quad (5)$$

A sample of the received Gaussian echo reflected by targets and its envelope is shown in Figures 8(a) and 8(b). The stronger reflection from target 2 in the HP compared to VP is observable in the reflected envelope. The processed data and antenna positions are the required input data for the image processing algorithm.

To examine the proposed method and to make a fair judgment about its performance, three images of the simulation scenario are reconstructed and shown in Figures 9(a)–9(c).

In all images, the dashed lines show the position of real abnormalities. Images obtained from the VP data show that target 1 was detected and positioned relative to the rear side of the phantom, as shown in Figure 9(a). Unlike target 1, target 2 is not easily observable in the VP image due to the target's small radar cross-section or RCS in vertical polarization which has caused the image to fail to detect the presence of target 2.

The reconstructed image based on HP (Figure 9(b)) has detected the location of target 2 since its shape shows a greater RCS in HP. However, there seems to be a spread in the location of target 1. This phenomenon is due to the fact that the monostatic RCS of target 1 varies for different positions of the radar transceiver which leads to receiving weak echoes in some angles. Consequently, the radar cannot collect enough samples from target 1 in HP.

The reconstructed image based on using the polarimetric information is shown in Figure 9(c). As one can see, this image has a powerful performance in revealing both targets compared to previous images. It also has higher quality and brings much more information about both

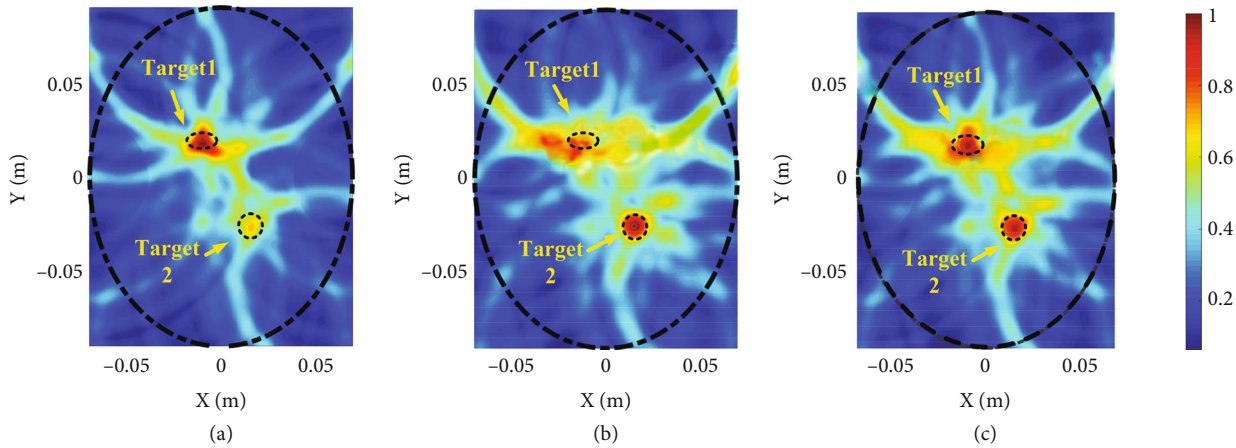

FIGURE 9: Reconstructed images of the patient's head phantom using (a) vertical data, (b) horizontal data, and (c) polarimetric data.

abnormality's locations and boundaries while VP and HP images could not show these details individually.

5. Conclusion

This article has proposed a transportable EM head imaging system based on polarimetric synthetic aperture radar to improve the probability of stroke detection for more sophisticated scenarios inside the human head. A compact, dual-polarized wideband, unidirectional, low-profile, body-matched antenna for the proposed imaging system is designed that covers the 1.2-4.5 GHz frequency band as the required EM sensor. The resulting system is a wearable biomedical sensor array with 16 antennas, whose performances and merits have been validated numerically in terms of imaging capabilities, by employing full-wave numerical simulations, 3D phantoms of the patient's head, two complex bleeding areas, and accurate modeling of the dual-pole antennas employed in the imaging system. The numerical simulation scenario demonstrates clearly that the introduced method can significantly increase the probability of revealing the region of the clot inside the head and the assumed reconstruction algorithm is robust against complex geometric bleeding shapes. This outcome is essential to developing future portable treatment systems to detect abnormalities inside the patient's head.

Data Availability

Data are available on request. Please contact the corresponding author.

Disclosure

This manuscript was written based on research done by a postgraduate student as part of his thesis at Shahed University.

Conflicts of Interest

The authors declare that they have no conflicts of interest.

References

[1] A. S. M. Alqadami, A. Trakic, A. E. Stancombe, B. Mohammed, K. Bialkowski, and A. Abbosh, "Flexible electromagnetic cap for head imaging," *IEEE Transactions on Biomedical Circuits and Systems*, vol. 14, no. 5, pp. 1097–1107, 2020.

[2] R. Scapaticci, J. Tobon, G. Bellizzi, F. Vipiana, and L. Crocco, "Design and numerical characterization of a low-complexity microwave device for brain stroke monitoring," *IEEE Transactions on Antennas and Propagation*, vol. 66, no. 12, pp. 7328–7338, 2018.

[3] A. S. M. Alqadami, K. S. Bialkowski, A. T. Mobashsher, and A. M. Abbosh, "Wearable electromagnetic head imaging system using flexible wideband antenna array based on polymer technology for brain stroke diagnosis," *IEEE Transactions on Biomedical Circuits and Systems*, vol. 13, no. 1, pp. 124–134, 2019.

[4] A. H. Naghavi, H. R. Hassani, and D. Oloumi, "Investigation and analysis of EM pulse propagation inside human head for high-resolution UWB elliptical SAR imaging," *IEEE Journal of Electromagnetics, RF and Microwaves in Medicine and Biology*, vol. 6, no. 4, pp. 485–493, 2022.

[5] D. Kurrant, J. Bourqui, C. Curtis, and E. Fear, "Evaluation of 3-D acquisition surfaces for radar-based microwave breast imaging," *IEEE Transactions on Antennas and Propagation*, vol. 63, no. 11, pp. 4910–4920, 2015.

[6] D. Oloumi, R. S. C. Winter, A. Kordzadeh, P. Boulanger, and K. Rambabu, "Microwave imaging of breast tumor using time-domain UWB circular-SAR technique," *IEEE Transactions on Medical Imaging*, vol. 39, no. 4, pp. 934–943, 2020.

[7] E. C. Fear, J. Bourqui, C. Curtis, D. Mew, B. Docktor, and C. Romano, "Microwave breast imaging with a monostatic radar-based system: a study of application to patients," *IEEE Transactions on Microwave Theory and Techniques*, vol. 61, no. 5, pp. 2119–2128, 2013.

[8] M. Rokunuzzaman, A. Ahmed, T. Baum, and W. S. T. Rowe, "A compact 3-D antenna for medical diagnosis of the human head," *IEEE Transactions on Antennas and Propagation*, vol. 67, no. 8, pp. 5093–5103, 2019.

[9] M. Persson, A. Fhager, H. D. Trefna et al., "Microwave-based stroke diagnosis making global prehospital thrombolytic

treatment possible," *IEEE Transactions on Biomedical Engineering*, vol. 61, no. 11, pp. 2806–2817, 2014.

[10] B. J. Mohammed, A. M. Abbosh, S. Mustafa, and D. Ireland, "Microwave system for head imaging," *IEEE Transactions on Instrumentation and Measurement*, vol. 63, no. 1, pp. 117–123, 2014.

[11] M. Rokunuzzaman, M. Samsuzzaman, and M. T. Islam, "Unidirectional wideband 3-D antenna for human head-imaging application," *IEEE Antennas and Wireless Propagation Letters*, vol. 16, pp. 169–172, 2016.

[12] M. Hopfer, R. Planas, A. Hamidipour, T. Henriksson, and S. Semenov, "Electromagnetic tomography for detection, differentiation, and monitoring of brain stroke: a virtual data and human head phantom study," *IEEE Antennas and Propagation Magazine*, vol. 59, no. 5, pp. 86–97, 2017.

[13] H. Trefna and M. Persson, "Antenna array design for brain monitoring," in *2008 IEEE Antennas and Propagation Society International Symposium*, pp. 1–4, San Diego, CA, USA, 2008.

[14] B. A. Mohammed, A. M. Abbosh, and P. Sharpe, "Planar array of corrugated tapered slot antennas for ultrawideband biomedical microwave imaging system," *International Journal of RF and Microwave Computer-Aided Engineering*, vol. 23, no. 1, pp. 59–66, 2013.

[15] A. Arayeshnia, S. Amiri, and A. Keshtkar, "Miniaturized on-body antenna for small and wearable brain microwave imaging systems," *International Journal of RF and Microwave Computer-Aided Engineering*, vol. 30, no. 4, article e22133, 2020.

[16] A. T. Mobashsher and A. Abbosh, "Development of compact directional antenna utilising plane of symmetry for wideband brain stroke detection systems," *Biomedical Technology*, vol. 50, no. 12, pp. 850-851, 2014.

[17] J. Liu and Q. Xue, "Broadband long rectangular patch antenna with high gain and vertical polarization," *IEEE Transactions on Antennas and Propagation*, vol. 61, no. 2, pp. 539–546, 2013.

[18] C. Gabriel, S. Gabriel, and E. Corthout, "The dielectric properties of biological tissues: parametric models for the dielectric spectrum of tissues," *Physics in Medicine and Biology*, vol. 41, no. 11, pp. 2271–2294, 2000.

[19] A. Arayeshnia, A. Keshtkar, and S. Amiri, "Realistic human head voxel model for brain microwave imaging," in *2017 Iranian Conference on Electrical Engineering (ICEE)*, pp. 1660–1663, Tehran, Iran, 2017.

[20] H. Bahramiabarghouei, E. Porter, A. Santorelli, B. Gosselin, M. Popović, and L. A. Rusch, "Flexible 16 antenna array for microwave breast cancer detection," *IEEE Transactions on Biomedical Engineering*, vol. 62, no. 10, pp. 2516–2525, 2015.

[21] I International and E Safety, *IEEE Standard for Safety Levels with Respect to Human Exposure to Radio Frequency Electromagnetic Fields, 3kHz to 300 GHz*, IEEE, 2006.

[22] R. Feghhi, D. Oloumi, and K. Rambabu, "Design and development of an inexpensive sub-nanosecond Gaussian pulse transmitter," *IEEE Transactions on Microwave Theory and Techniques*, vol. 67, no. 9, pp. 3773–3782, 2019.

[23] D. Oloumi, K. K.-M. Chan, P. Boulanger, and K. Rambabu, "SAGD process monitoring in heavy oil reservoir using UWB radar techniques," *IEEE Transactions on Microwave Theory and Techniques*, vol. 64, no. 6, pp. 1884–1895, 2016.

[24] D. Oloumi, J.-W. Ting, and K. Rambabu, "Design of pulse characteristics for near-field UWB-SAR imaging," *IEEE Transactions on Microwave Theory and Techniques*, vol. 64, no. 8, pp. 2684–2693, 2016.